mlk00 | ACSJCA | JCA10.0.1465/W Unicode | research.3f (R3.6.i5 HF01:4227 | 2.0 alpha 39) 2014/03/19 08:04:00 | PROD-JCAVA | rq_3724906 | 7/14/2014 15:39:03 | 10 | JCA-DEFAULT

THE JOURNAL OF PHYSICAL CHEMISTRY B

Article

pubs.acs.org/JPCB

# Observation of Vibrational Energy Exchange in a Type-III Antifreeze Protein

S. Lotze,*,[†] L. L. C. Olijve,[‡,¶] I. K. Voets,[‡,¶] and H. J. Bakker[†]

[†]FOM-Institute for Atomic and Molecular Physics AMOLF, Science Park 104, 1098 XG Amsterdam, The Netherlands

[‡]Laboratory for Macromolecular and Organic Chemistry, Department of Chemical Engineering and Chemistry and [¶]Institute for Complex Molecular Systems, Eindhoven University of Technology, P.O. Box 513, 5600 MB Eindhoven, The Netherlands

*S* *Supporting Information*

**ABSTRACT:** We performed time- and polarization-resolved pump−probe and two-dimensional infrared (2D-IR) experiments to study the dynamics of the amide I vibration of a 7 kDa type-III antifreeze protein. In the pump−probe experiments, we used femtosecond mid-infrared pulses to investigate the vibrational relaxation dynamics of the amide mode. The transient spectra show the presence of two spectral components that decay with different lifetimes, indicative of the presence of two distinct amide subbands. The 2D-IR experiments reveal the coupling between the two bands in the form of cross-peaks. On the basis of previous work by Demirdöven et al. (*J. Am. Chem. Soc.* **2004**, *126*, 7981−7990), we assign the observed bands to the two infrared-active modes $\alpha(-)$ and $\alpha(+)$ found in protein $\beta$-sheets. The amplitudes of the cross-peak were found to increase with delay time, indicating that the cross-peaks originate from population transfer between the coupled amide oscillators. The time constant of the energy transfer was found to be 6−7 ps.

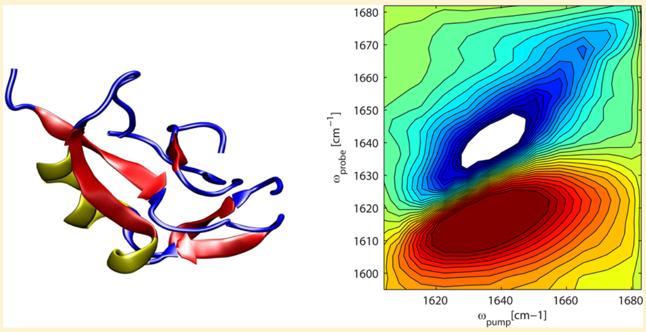


## 1. INTRODUCTION

Among the various normal modes of the protein backbone, the amide I band forms a particularly sensitive marker for secondary structural elements. The vibration consists primarily of the displacement of the carbonyl group of the amide moiety with additional contributions from CN-streching and NH-bending.[1] The latter contribution is responsible for a slight shift of the amide I resonance frequency upon isotopic exchange from hydrogen to deuterium (denoted as amide I′). Amide oscillators are known to be coupled by electrostatic interactions, leading to the formation of vibrational excitons.[2,3] Depending on the degree of structural disorder, these excitons can be partially delocalized over several residues of the peptide chain. Hochstrasser and co-workers were the first to investigate the signature of the excitonic states of the amide I′ band with nonlinear infrared spectroscopy.[4] They found that vibrational excitations are delocalized between coupled sets of amide oscillators over a length of ~8 Å.

Over the past years, two-dimensional infrared (2D-IR) spectroscopy has become an extremely valuable tool for the study of the amide I vibration of proteins and peptides, owing to its sensitivity to fast dynamics occurring on femto- to picosecond time scales. Most 2D-IR studies have focused on the analysis of line shapes and coupling patterns, and many insightful observations about the structure and the conformational dynamics have been obtained.[5−12] In combination with theoretical modeling and residue-specific isotope labeling, mechanistic models and structure−function relationships have been devised for systems as complex as the M2 proton channel,[5,11] membrane-associated peptides,[6] and dimers of transmembrane helices[12] based on 2D-IR spectra. The aforementioned studies have mainly been performed for a fixed timing of the pulses in the 2D-IR pulse sequence, and relatively few studies have focused on the dynamics of the amide mode.[13−16] In a recent study by Middleton et al., it was found that the vibrational lifetime of the amide I′ mode is correlated with the degree of structural disorder.[13] Hamm and co-workers have observed the breaking and re-formation of hydrogen bonds between the amide groups of *N*-methylacetamide and the hydroxyl groups of methanol.[14] The same group has also studied the energy-transfer dynamics between the amide oscillators of small peptides embedded in different environments.[15,16]

In this paper, we report on a study of the response of the amide I′ vibration of a 67 residue type-III antifreeze protein (AFPIII) from ocean pout (*Macrozoarces americanus*) with linear and nonlinear infrared spectroscopy. Antifreeze proteins are a class of proteins that are found in the body fluids of organisms that need to survive at subzero temperatures and are known to act as cryoprotectants by lowering the freezing point of aqueous solution with respect to the melting point.[17] We have applied polarization-resolved infrared pump−probe

**Received:** April 9, 2014
**Revised:** July 9, 2014





dx.doi.org/10.1021/jp503481e | *J. Phys. Chem. B* XXXX, XXX, XXX−XXX

experiments using femtosecond pulses to the study of vibrational relaxation dynamics and, in addition, performed delay-dependent 2D-IR experiments using narrow-band excitation pulses to obtain insight into the energy-transfer dynamics of the amide I′ band of AFPIII. The results strongly suggest the presence of intramolecular $\beta$-sheets in agreement with the X-ray crystal structure, demonstrating the sensitivity of 2D-IR for flexible structural elements invisible by commonly employed spectroscopic tools to probe the protein structure in solution such as circular dichroism spectroscopy.[18−20]

## 2. EXPERIMENTAL SECTION

**2.1. Nonlinear Infrared Spectroscopy.** We measure the vibrational relaxation dynamics of the amide I′ vibration of 1.4 mM solutions of AFPIII dissolved in a $D_2O$ buffer (containing 150 mM NaCl, 20 mM tris(hydroxymethyl) aminomethane). $D_2O$ is used instead of $H_2O$ to avoid the absorption of the mid-infrared pulses by the bending mode of $H_2O$. The femtosecond pulses required for this study are generated by a series of nonlinear frequency conversion processes that are pumped with the pulses of a commercial Ti:sapphire regenerative amplifier (Coherent Legend Elite Duo). The amplifier system delivers 50 fs pulses centered at around 800 nm with a pulse energy of 7 mJ. About 4.5 mJ of the amplifier output is used to pump a white-light-seeded optical parametric amplifier (OPA, HE-TOPAS, Light Conversion) based on BBO ($\beta$-barium borate), generating signal and idler pulses at wavelengths around 1480 and 1852 nm, respectively. The mid-IR pulses are generated by mixing the signal and idler pulses in a type-I difference frequency mixing process (DFG) in a silver thiogallate crystal ($AgGaS_2$, cut-angle $\Theta = 39°$). The resulting mid-IR pulses have a wavelength of 5.9 $\mu$m, an energy of 30 $\mu$J, and a spectral width of approximately 300 $cm^{-1}$. To avoid absorption of the infrared pulses by ambient air, the setup is purged with nitrogen during the experiment. The pulse length at the sample position is determined by two-photon absorption in an InAs wafer and inferred to be ∼100 fs. We use the pulses in a pump−probe experiment. Small portions (∼0.3%) of the mid-IR pulses are split off by means of two wedged $CaF_2$ windows, and the front reflections are used as probe and reference beams. The transmitted light is used as the pump beam. The probe beam is sent over a motorized delay stage to vary the time delay between the pump and probe pulses. The pump, probe, and reference beams are focused into the sample by a gold-coated off-axis parabolic mirror ($f$ = 75 mm) and recollimated by an identical mirror. The pump and probe foci are spatially overlapped in the sample. The transmitted probe and reference beams are focused onto the entrance slit of an imaging monochromator (Lot-Oriel MSH 302) with an off-axis parabolic mirror ($f$ = 100 mm) and frequency-dispersed on the two lines of a 2 × 32 mercury−cadmium−telluride (MCT, Infrared Associates) array. The reference beam is used for a pulse-to-pulse correction of the intensity fluctuations. The pump beam is chopped at a frequency of 500 Hz to detect only the pump-induced absorption changes in the probe light as a function of pump−probe delay. A zero-order $\lambda/2$ plate is used to set the polarization of the pump beam at 45° relative to that of the probe light. Behind the sample cell, a rotatable wire grid polarizer is placed to select the polarization component of the probe beam parallel or perpendicular to the pump beam. From the parallel ($\Delta\alpha_{\parallel}$) and perpendicular ($\Delta\alpha_{\perp}$) components of the transient absorption changes, the isotropic signal is constructed

$$\Delta\alpha_{\text{iso}}(\omega, t) = \frac{1}{3}(\Delta\alpha_{\parallel}(\omega, t) + 2\Delta\alpha_{\perp}(\omega, t)) \quad (1)$$

The signal constructed in this way is unaffected by orientational effects and solely reflects the vibrational relaxation. In addition, we also construct the time-dependent anisotropy parameter $R(\omega,t)$

$$R(\omega, t) = \frac{\Delta\alpha_{\parallel}(\omega, t) - \Delta\alpha_{\perp}(\omega, t)}{3\Delta\alpha_{\text{iso}}(\omega, t)} \quad (2)$$

The anisotropy parameter is proportional to the second-order orientational correlation function of the transition dipole moment and reflects the kinetics of the depolarization of the excitation. Thus, performing the experiment in a polarization-resolved manner allows one to measure simultaneously the vibrational relaxation kinetics and the decay of the orientational correlation of the amide I′ mode. Relaxation of the initially excited amide I′ oscillators as well as direct absorption of the pump light by the high-frequency shoulder of the $D_2O$ band centered at 1500 $cm^{-1}$ leads to the rise of a thermal signal in the pump−probe spectra. In order to describe the kinetics of this process in a model-free approach, we have measured the pump-induced shift of the OD-stretch band using a second, independently tunable OPA-DFG stage, generating probe pulses in resonance with the shoulder of the OD-stretch absorption band of the solvent (∼2200 $cm^{-1}$). The pump pulse remains tuned to the amide I′ vibration. The kinetics obtained from this experiment are used to subtract the time-dependent thermal signal from the pump−probe data set prior to further analysis. In this procedure, we have implicitly assumed that the time dependence of thermal effects is identical for all modes in the sample.

In addition, we perform 2D-IR experiments, implemented as a spectral hole-burning experiment. Here, we excite a subensemble of amide I′ oscillators with a narrow-band excitation pulse and follow its spectral evolution with a broad-band probing pulse. To generate excitation pulses with the desired small bandwidth (10 $cm^{-1}$), we insert a home-built Fabry−Perot etalon, consisting of two parallel, partially transparent mirrors (reflectivity $R$ = 90%) in the path of the pump beam. The time domain shape of the resulting pulses is approximately a single-sided exponential with a $1/e$ decay time of 500 fs. The center frequency of the narrow-band excitation pulses can be varied by adjusting the spacing between the two mirrors. In practice, this is achieved by placing one of the two mirrors on a piezo-driven mirror mount. The spectral profile of the excitation pulse is monitored by directing a small fraction of the pump light into the spectrometer and imaging it on the MCT detector. The signal from the MCT detector is used in an automated feedback routine to drive the piezo actuators, thereby allowing one to tune the spectrally narrow excitation pulse to the desired center frequency and thus to scan the pulse over the entire amide I′ absorption band. During all experiments, the samples are held between two $CaF_2$ windows separated by Teflon spacers with a thickness in the range between 25 and 50 $\mu$m. The temperature of the sample is set by a thermoelectric module and actively stabilized over the course of the experiment by a programmable temperature controller (PTC 10, Stanford Research Systems), driven by in-house designed software. For experiments below 8 °C, the samples are rotated during the measurement to ensure that each laser shot probes a fresh portion of the sample so as to avoid steady-state heating in the focus.

## 3. EXPERIMENTAL RESULTS AND INTERPRETATION

**3.1. Isotropic Transient Spectra.** Figure 1 shows the transient absorption changes of the amide I′ band of AFPIII.

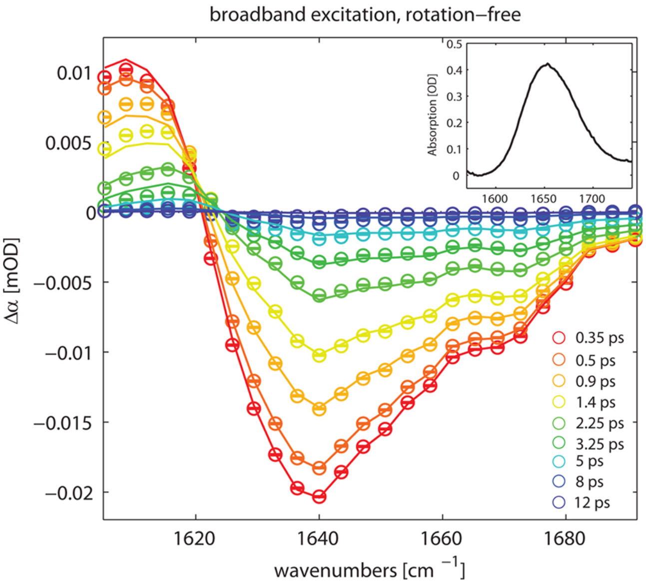


**Figure 1.** 1D pump−probe data of AFPIII obtained under broad-band excitation. The sample thickness used in the experiment was 50 μm. The open circles represent the data points after subtraction of the time-dependent rise of the thermal signal. The solid lines represent a fit to the model outlined in the text. The inset shows the linear absorption spectrum of the sample after subtraction of the solvent background.

The spectrally broad excitation pulses used in this experiment have sufficient bandwidth to cover the entire amide I′ absorption band. The spectra show a negative response that peaks at 1640 cm$^{-1}$, originating from the bleaching of the ground state ($\nu$ = 0) and stimulated emission from the first excited state ($\nu$ = 1) of the amide I′ mode. The positive feature in the transient spectrum observed at frequencies < 1620 cm$^{-1}$ originates from excited-state absorption ($\nu = 1 \rightarrow 2$). The signal at delay times > 20 ps has a flat and featureless shape (not shown here) and originates from the shift of the solvent background due to heating. The contribution from this signal has been subtracted from the data in Figure 1, as outlined in the Experimental Section. In addition to the thermal signal that originates from the solvent, also a local, transient heating effect may be present in the pump−probe data of Figure 1. We have studied the influence of heating on the amide I′ band by measuring solvent-corrected temperature difference absorption spectra, which are shown in Figure S1 of the Supporting Information. We find that an increase in temperature leads to a blue shift of the amide I′ band, accompanied by a decrease in absorption cross section, which in the transient absorption spectrum would lead to a bleach in the frequency region from 1620 to 1660 cm$^{-1}$ and a weak induced absorption in the region > 1660 cm$^{-1}$.

It is worth noting the difference in spectral shapes between the linear absorption spectrum of AFPIII shown in the inset of Figure 1 and the nonlinear pump−probe spectrum. In the FTIR spectrum, the amide I′ band appears as a nearly Gaussian-shaped absorption line without shoulders or side lobes. The slight asymmetry might in fact be caused by imperfect subtraction of the solvent background. In contrast, the bleaching signal of the transient spectra in Figure 1 exhibits a clear additional shoulder at around 1670 cm$^{-1}$, which is thus not observed in the linear spectrum. The difference in intensity distribution can be understood from the dependence of the signal amplitude on the absorption cross section, which is linear in the case of the FTIR spectrum but scales quadratically with the absorption cross section in the pump−probe spectrum. In Figure 2, we plot the isotropic transient absorption changes

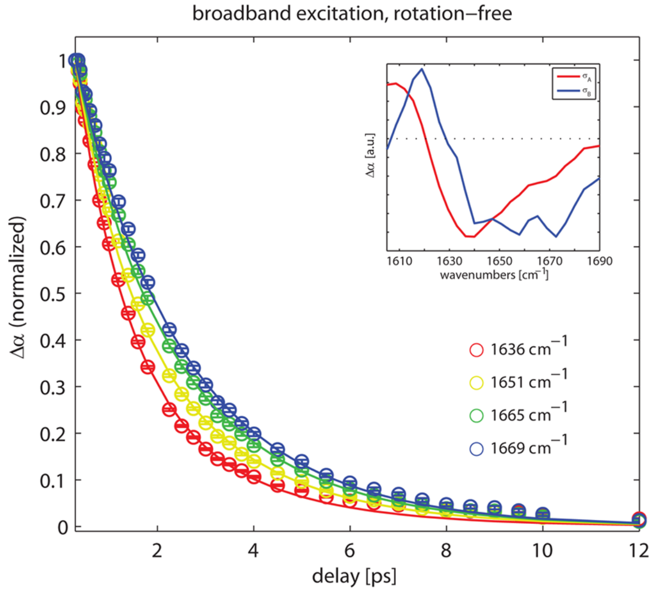


**Figure 2.** Transient absorption change obtained under broad-band excitation conditions at different detection frequencies. The data have been normalized to the signal at 300 fs. Open circles represent the data points obtained after subtraction of the thermal signal, as described in the text. The solid lines represent the fit to the kinetic model outlined in the text, and the inset shows the spectral signatures of the excited states obtained with the fit.

obtained from the broad-band excitation experiments at four different detection frequencies. To avoid any unwanted contributions arising from coherent coupling between pump and probe pulses during the time overlap of the pulses[21,22] or perturbed free induction decay effects,[23,24] we analyze the population relaxation only after a pump−probe delay of 300 fs. The data have been normalized to the maximum signal to facilitate a comparison of the dynamics. The population decay of the amide I′ vibration has a pronounced frequency dependence, which points to the presence of more than one subensemble of amide oscillators within the absorption band. We find the decay to slow down with increasing frequency, which is consistent with the observation of a blue shift of the transient spectrum in Figure 1 with increasing delay time.

We describe the data set $\Delta\alpha(\omega,t)$ with a model that contains two excited states decaying with different lifetimes to a common ground state. The spectral signature of the excited states that we extract from the fit are depicted in the inset of Figure 2. We find the lower-frequency component of the spectrum to decay with a lifetime of $T_1^a$ of 1.09 ps, whereas the high-frequency component exhibits a longer lifetime $T_1^b$ of 3.21 ps. The details of the fitting procedure are described in section 3.3.

More detailed information on the structural origin of the two components can be obtained from a 2D-IR spectroscopic experiment, in which the coupling between different sets of

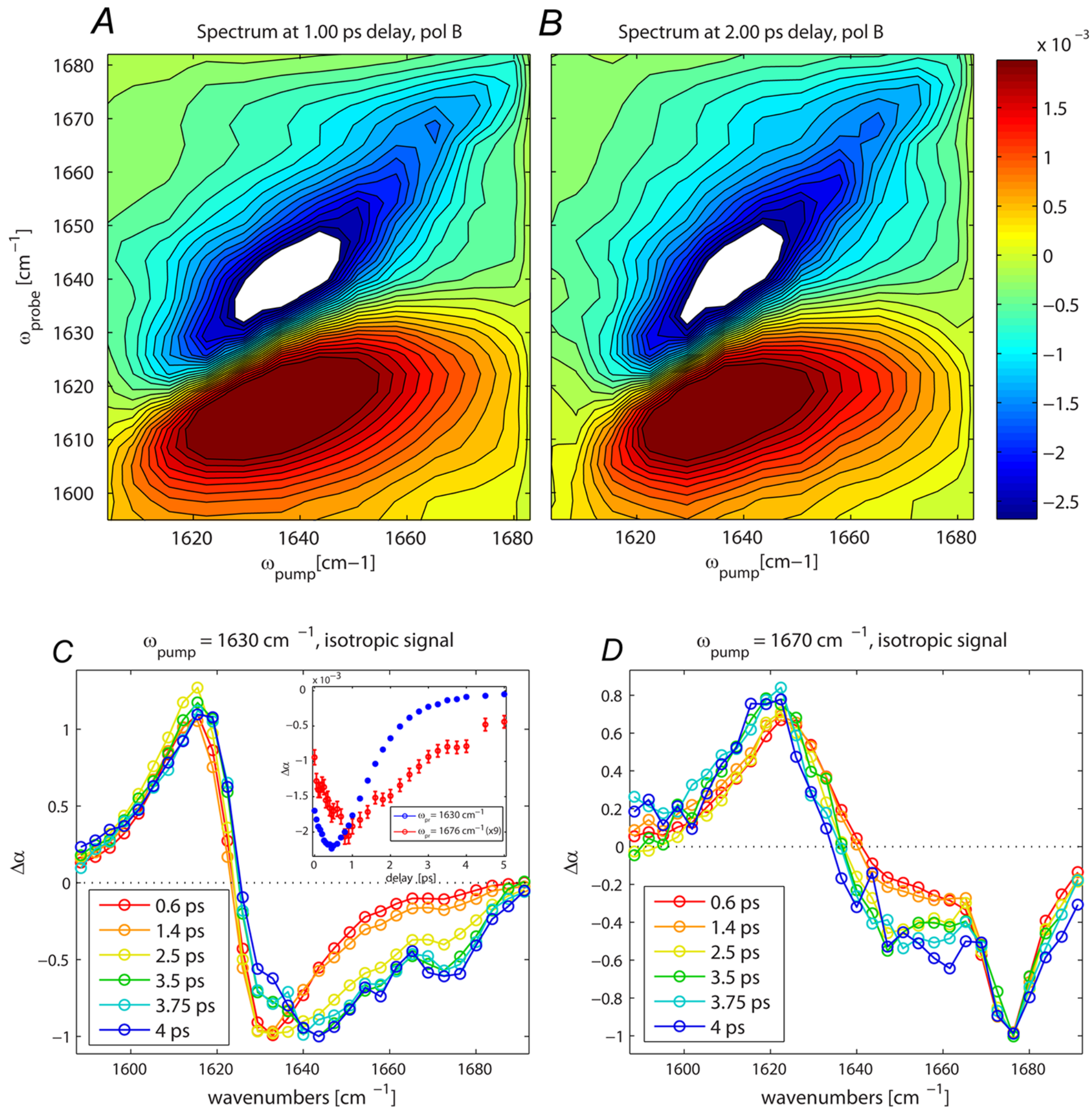


**Figure 3.** 2D-IR spectra of the amide I′ region of AFPIII, obtained at a delay time of (a) 1 and (b) 2 ps measured with perpendicular polarization of the pump and probe pulses. The spectra have been generated from a series of narrow-band excitation experiments with 12 different pump positions. Negative absorption signals are depicted as blue, and positive absorption signals are in red. The contours are equally spaced between +70 and −70% of the maximum bleaching signal. (c,d) Cuts through the isotropic part of the 2D-IR spectrum for excitation frequencies $\omega_{pump}$ = 1630 cm$^{-1}$ (c) and $\omega_{pump}$ = 1670 cm$^{-1}$ (d), normalized to the minimum of the bleaching signal. The inset in (c) shows the delay traces of the diagonal peak ($\omega_{probe}$ = 1630 cm$^{-1}$) and the off-diagonal signal ($\omega_{probe}$ = 1670 cm$^{-1}$) for $\omega_{pump}$ = 1630 cm$^{-1}$. The off-diagonal signal is magnified by a factor of 9 for clarity.

amide modes reveals itself in the form of cross-peaks. As outlined in the Experimental Section, we have implemented 2D-IR spectroscopy in the form of a hole-burning experiment, in which we make use of tunable, spectrally narrow excitation pulses in combination with broad-band probing pulses.[4,15,25,26]

In Figure 3, we show 2D-IR spectra obtained at delays of 1 (Figure 3a) and 2 ps (Figure 3b) measured with a probe pulse with a polarization perpendicular to that of the pump. The negative bleaching/stimulated emission signal shows a pronounced elongation along the diagonal in both spectra. This correlation between excitation and probing frequency reflects inhomogeneous broadening, which is static on the time scales shown here (1−2 ps). In addition, we observe a ridge in the negative signal above the diagonal at $\omega_{probe}$ = 1670 cm$^{-1}$, which becomes more pronounced with increasing delay time (Figure 3b).

To visualize the time evolution of the spectrum, we plot in Figure 3c and d cuts through the 2D spectrum at excitation frequencies of $\omega_{pump}$ = 1630 cm$^{-1}$ and $\omega_{pump}$ = 1670 cm$^{-1}$ at delay times ranging from 0.6 to 4 ps, normalized to the minimum of the bleaching signal. The thermal level has been subtracted in the same way as described above for the experiments under broad-band excitation. Upon excitation of the amide oscillators at either position, a delayed rise of a bleaching signal is seen in the off-diagonal region, pointing to the presence of rising cross-peaks in these regions of the 2D spectrum. The inset in Figure 3c shows the delay traces at $\omega_{probe}$ = 1630 cm$^{-1}$ (diagonal signal) and $\omega_{probe}$ = 1670 cm$^{-1}$ (off-diagonal signal). The plot clearly shows that the off-diagonal signal peaks at a later delay time than the diagonal signal and that both signals decay with different lifetimes. The signal at $\omega_{probe}$ = 1670 cm$^{-1}$ must therefore constitute a cross-peak that results from the exchange of population with the


dx.doi.org/10.1021/jp503481e | J. Phys. Chem. B XXXX, XXX, XXX−XXX

directly excited amide oscillators. The fact that the ingrowing signal in the region > 1660 $cm^{-1}$ corresponds to a negative absorption change (bleaching signal) excludes the possibility that this contribution would originate from a heating effect on the amide I′ mode as (local) heating would cause a positive signal (induced absorption) in this frequency range (see Figure S1 of the Supporting Information). In Figure 3d, the grow-in of a bleaching signal in the region $\omega_{probe}$ = 1630−1660 $cm^{-1}$ following excitation at 1670 $cm^{-1}$ is observed. This bleaching is partially compensated for by the positive-valued-induced 1 → 2 absorption. The rise of this off-diagonal bleaching signal results from population transfer from the directly excited high-frequency mode at 1670 $cm^{-1}$ to amide oscillators at lower frequencies.

Recently, a systematic study of the 2D-IR spectroscopic signatures of different structural elements of proteins and peptides has been performed by the Tokmakoff group.[8] In this study, it was shown that the two infrared-active vibrational modes associated with antiparallel $\beta$-sheet elements, denoted as $\alpha(+)$ and $\alpha(-)$, are strongly coupled and give rise to a distinct cross-peak in the 2D-IR spectrum. On the basis of this work, we assign the two components that we observe at $\omega \approx 1630$ and 1670 $cm^{-1}$ in the 2D-IR spectra of AFPIII to the $\alpha(-)$ and $\alpha(+)$ modes of the $\beta$-sheets, respectively. The $\alpha(+)$ and $\alpha(-)$ are collective modes that consist primarily of the in-phase movement of amide I′ oscillators on adjacent strands, leading to a delocalized mode with a transition dipole moment perpendicular to the direction of the $\beta$-strands ($\alpha(-)$) and the in-phase movement of neighboring oscillators within one strand ($\alpha(+)$), forming a mode with a transition dipole moment approximately parallel to the strands. The character of these modes is illustrated in Figure 8b.

### 3.2. Kinetic Modeling of the Exchange.

With the findings in the previous paragraph in mind, we return to the kinetic analysis of the broad-band pump−probe data. To account for the energy transfer within the amide I′ absorption band that was observed in the 2D-IR spectra, we employ a kinetic model that is outlined schematically in Figure 4 to fit the isotropic pump−probe data set $\Delta\alpha_{iso}(\omega,t)$. We assume that the data set can be described by the product of the time-dependent populations $N_i(t)$ of the states involved in the relaxation scheme and their associated spectral signatures $\sigma_i$

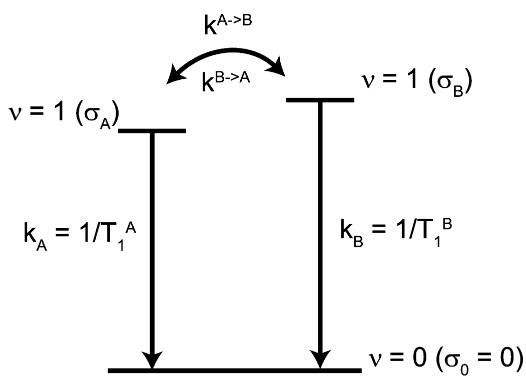


**Figure 4.** Rate model employed to fit the isotropic pump−probe data set $\Delta\alpha_{iso}(\omega,t)$. The rates of population transfer between the two excited states are constrained by the detailed balance condition $k_{A\rightarrow B}/k_{B\rightarrow A} = e^{-\Delta E/kT}$. A detailed description of the rate equations can be found in the Appendix.

$$\Delta\alpha_{iso}(\omega, t) = N_A(t)\cdot\sigma_A + N_B(t)\cdot\sigma_B + N_0(t)\cdot\sigma_0 \quad (3)$$

The subscripts A, B, and 0 denote the two excited states included in the model of Figure 4 and the ground state, respectively. It should be noted that the spectra $\sigma_i$ represent difference spectra with the absorption spectrum of the ground state. At later delay times, the transient spectrum will be formed by a thermal difference spectrum representing the change in absorption of the ground state induced by the thermalization of the vibrational excitation. However, this contribution is already eliminated by the subtraction of the rising thermal difference spectrum from the data set, as outlined in the Experimental Section. From a least-squares fit, we find a rate of energy transfer from the higher-lying state to the lower-energy state of $k_{B\rightarrow A} = (7.1 \pm 0.2\ ps)^{-1}$ and rates of relaxation to the ground state of $k_A = 1/T_1^A = (1.09 + 0.01\ ps)^{-1}$ and $k_A = 1/T_1^B = (3.21 \pm 0.07\ ps)^{-1}$. Figure 5 shows the temperature dependence of the rate constants obtained from the least-squares fit, ranging from 2 to 20 °C. We find that the exchange rate $k_{B\rightarrow A}$ as well as the vibrational relaxation rates $k_A$ and $k_B$ are essentially temperature-independent over the investigated range. The associated spectral signatures of the excited states $\sigma_A$ and $\sigma_B$ that we extract from the fit are depicted in the inset of Figure 2.

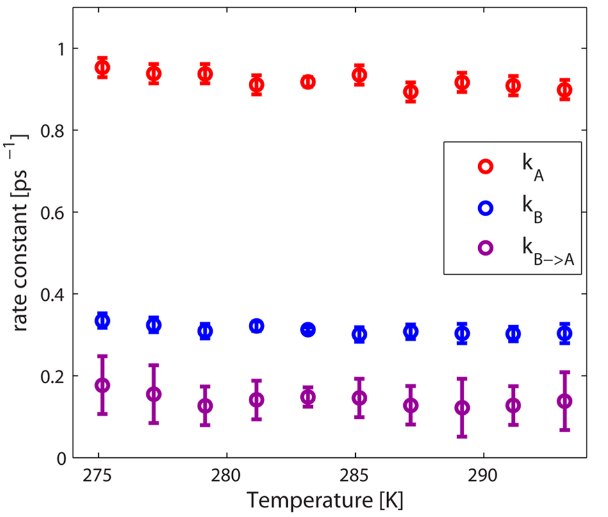


**Figure 5.** Rate constants obtained from a fit of the isotropic data set $\Delta\alpha_{iso}(\omega,t)$ to the model of Figure 4 for different sample temperatures between 2 and 20 °C. Both the vibrational relaxation rates $1/T_1^A$ and $1/T_1^B$ of the two amide I′ subbands as well as the exchange rate $k_{B\rightarrow A}$ show only minor variation with temperature.

We employ the rate constants outlined above to perform a model calculation of the time evolution of the 2D-IR spectrum. The results of these calculations are presented in Figure 6 for two different excitation frequencies of $\omega_{pump}$ = 1630 $cm^{-1}$ and $\omega_{pump}$ = 1670 $cm^{-1}$. The calculated spectra are to be compared with the experimental data in Figure 3c and d. The calculations are based on fitting the isotropic transient spectra at earliest delay times ($\tau$ = 0.6 ps) obtained for $\omega_{pump}$ = 1630 $cm^{-1}$ and $\omega_{pump}$ = 1670 $cm^{-1}$ with a sum of Lorentzians and subsequently calculating the time evolution of these two components with the kinetic model and the rate constants outlined in the previous paragraphs. The peak positions and the line widths of the Lorentzians are presented in Table S1 of the Supporting Information. The spectra obtained for $\omega_{pump}$ = 1630 $cm^{-1}$ are in excellent agreement with the transient spectra in Figure 3c. The


dx.doi.org/10.1021/jp503481e | J. Phys. Chem. B XXXX, XXX, XXX−XXX

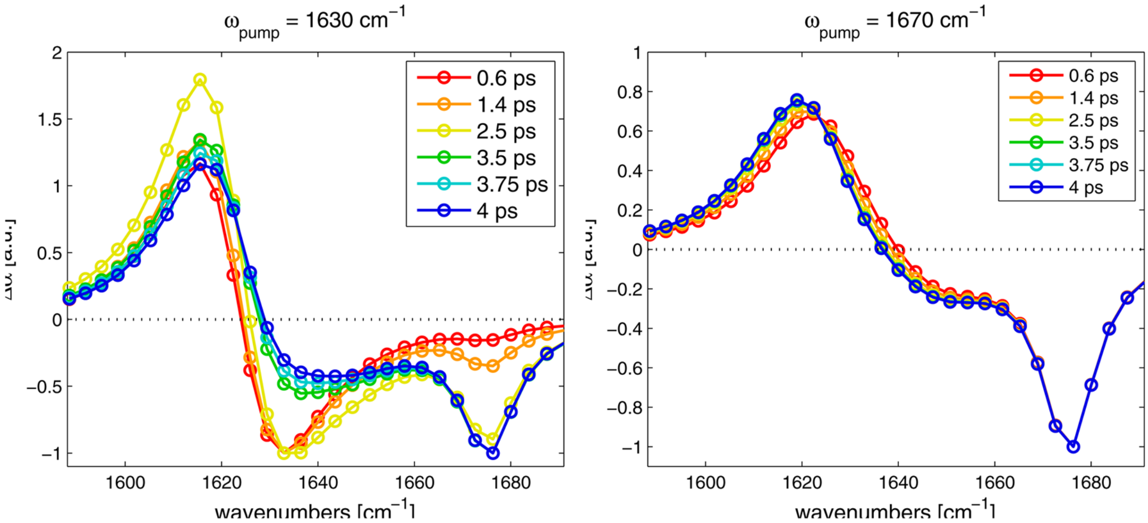


**Figure 6.** Calculated delay time dependence of cuts through the 2D-IR spectrum for excitation frequencies of $\omega_{pump}$ = (A) 1630 and (B) 1670 $cm^{-1}$. The results are directly to be compared with the experimental data in Figure 3c,d.

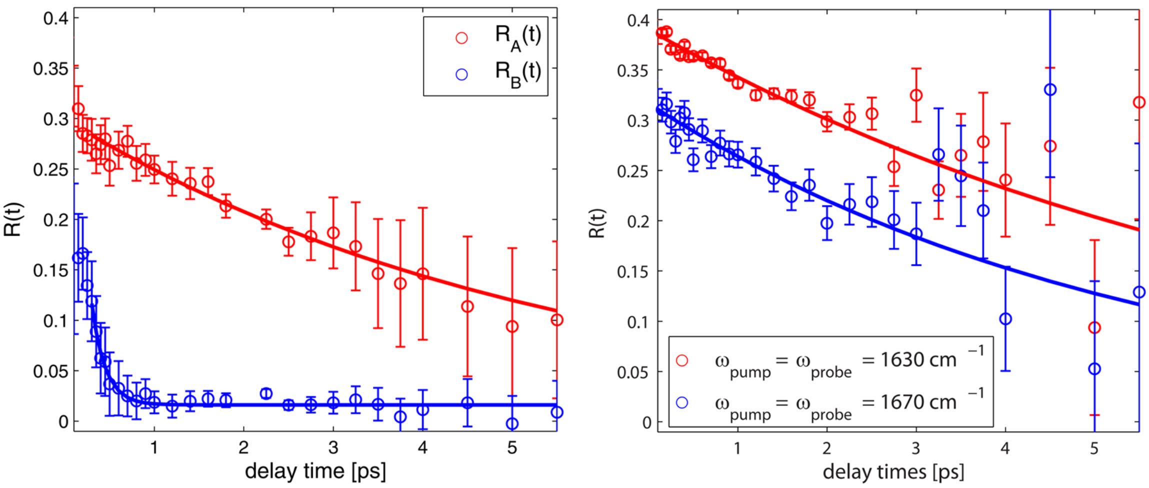


**Figure 7.** (A) Anisotropy decays obtained from a decomposition of the polarization-resolved broad-band pump−probe data sets $\Delta\alpha_{\parallel}(\omega,t)$ and $\Delta\alpha_{\perp}(\omega,t)$. (B) Anisotropy decays of the diagonal signal of the 2D-IR spectrum for narrow-band excitation $\omega_{pump}$ = 1630 and 1670 $cm^{-1}$. The solid lines are exponential fits to the data.

delayed rise of the bleaching signal in the range of $\omega_{probe}$ = 1640−1680 $cm^{-1}$ as well as the small blue shift of the induced absorption signal with increasing delay time are well reproduced. It should be noted that also the initial increase and subsequent decay of the induced absorption signal with a maximum at intermediate delay times ($\tau$ = 2.5 ps, yellow curves in Figures 3c and 6a) is well reproduced by our model. The agreement of the calculations for $\omega_{pump}$ = 1670 $cm^{-1}$ in Figure 6b with the experimental data of Figure 3d is less good; however, the main features and trends of the time-dependent transient spectra can be reproduced. The transient red shift of the induced absorption and the rise of the bleaching signal in the region of $\omega_{probe}$ = 1640−1665 $cm^{-1}$ is accounted for by the calculations, albeit that the latter feature is less pronounced in the calculations than that in the experimental data. The overall less good agreement of the model calculations with the experimental data for $\omega_{pump}$ = 1670 $cm^{-1}$ than those for $\omega_{pump}$ = 1630 $cm^{-1}$ might be due to the presence of additional spectral equilibration after narrow-band excitation at 1670 $cm^{-1}$, which is not included in the present model. The narrower width of the bleaching signal immediately after excitation at 1670 $cm^{-1}$ ($\tau$ = 0.6 ps in Figure 3d) when compared to the initial bleach after excitation at 1630 $cm^{-1}$ ($\tau$ = 0.6 ps in Figure 3c) suggests that a slow spectral diffusion process affects the time evolution of the transient spectra stronger in the case of excitation of the $\alpha(+)$ band at 1670 $cm^{-1}$, for which a narrow spectral hole of ~10 $cm^{-1}$ burned, than that in the case of pumping at 1630 $cm^{-1}$, where the initial bleach has a width of approximately 20 $cm^{-1}$.

**3.3. Anisotropy Dynamics of the Pump−Probe Experiments.** The spectral signatures can be used together with the polarization-resolved data sets $\Delta\alpha_{\parallel}(\omega,t)$ and $\Delta\alpha_{\perp}(\omega,t)$ to construct the time-dependent anisotropy decays for both individual bands, as outlined in detail in the Appendix.

The anisotropy curves obtained in this way are shown in Figure 7. We find that the anisotropy curve of the high-frequency band $R_B(t)$ exhibits a large drop within the first 500 fs, leading to an almost complete decay. In contrast, the anisotropy of the low-frequency band, $R_A(t)$, shows a much slower decay on a time-scale of several picoseconds. We find that the decay of $R_A(t)$ can be well described by a single exponential with a decay rate of $1/\tau = (5.5\ ps)^{-1}$.

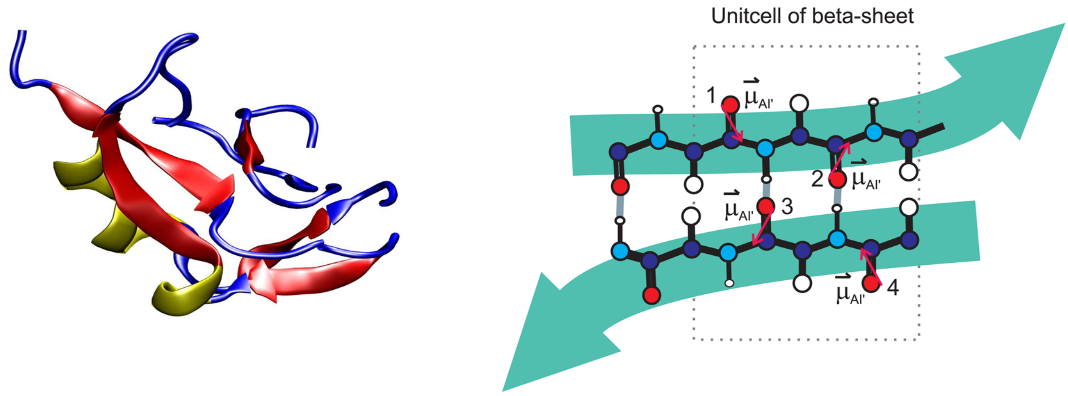


**Figure 8.** (A) Crystal structure of type-III AFP determined by Antson et al.[19] (pdb code 1HG7). The strands of the $\beta$-sheets are represented in red, random coil elements are in blue, and helices are in yellow. (B) Schematic representation of the infrared-active collective vibrations of antiparallel $\beta$-sheets according to ref 8. Red arrows indicate the direction of the transition dipole moment of the amide I′ mode of the individual peptide moieties 1−4. Both the $\alpha(-)$ and $\alpha(+)$ modes correspond to the out-of-phase stretching movement of the (1,4) and (2,3) pairs of amide oscillators on adjacent $\beta$-strands. The $\alpha(+)$ mode is associated with the in-phase movement of neighboring oscillators (pairs (1,3) and (2,4), respectively), whereas the $\alpha(-)$ mode corresponds to the out-of-phase movement of these oscillators.

In Figure 7b, we show the anisotropy decays of the diagonal signals of the 2D spectrum. Interestingly, neither of the anisotropy curves in Figure 7b shows a similar rapid decay as observed for the $R_B(t)$ curve in Figure 7a. Instead, both curves decay on a time scale comparable to $R_A(t)$ in Figure 7a. The different dynamics of the anisotropy decays in broad-band pump−probe experiments compared to 2D-IR experiments has its origin in the exchange of population between the two modes considered in our model. In the 2D-IR experiment, the spectrally selective excitation pulse creates population in only one of the excited states. The excited-state population can either decay to the ground state ($T_1$ relaxation) or transfer population to the other mode (cross-relaxation). Both processes lead to a decay of the isotropic pump−probe signal of the initially excited mode, that is, of the diagonal signal in the isotropic 2D spectrum, while at the same time leaving the anisotropy of the signal unaffected. The anisotropy of each probed amide I′ vibration can only decay due to molecular reorientation or if another excited vibration with a different orientation, that is, the other amide I′ mode, changes its character (frequency) to that of the probed vibration.

The situation outlined above for the narrow-band excitation 2D-IR experiments contrasts the situation encountered in the pump−probe experiments with broad-band excitation pulses. The spectrally broad pump pulse generates excited-state population in both modes, with the ratio of population in the $\nu = 1$ states being determined by the cross sections of the two modes. The excitation of both modes enables the exchange of population between the two excited, differently oriented amide I′ modes, thereby opening up an efficient loss channel for the anisotropy. Considering that the cross section of the lower-frequency band $\sigma_A$ is higher than that of $\sigma_B$, mode A will be more strongly excited than mode B. As a result, the exchange will have a much stronger effect on the anisotropy of mode B than that on the anisotropy of mode A, thus likely causing the observed fast decay in the anisotropy curve $R_B$ shown in Figure 7a.

## 4. DISCUSSION

The splitting of the amide I′ band and the accompanying formation of cross-peaks in the 2D-IR spectrum are highly characteristic for antiparallel $\beta$-sheets.[8,27] Structurally disordered segments do not feature this distinctive line shape behavior. Therefore, the two amide I′ modes as observed in our experiment appear to be dominated by $\beta$-sheet character, thus supporting an assignment to $\alpha(-)$ and $\alpha(+)$ modes. The prevalence of $\beta$-sheet character in the amide I′ response is in agreement with the crystal structure of AFPIII that has been determined by Anston et al.[19] and is shown in Figure 8A. Nevertheless, in view of the structure of AFPIII proteins, it is likely that one or even both of the spectral components obtained in the analysis (inset of Figure 2) contains a contribution from random coil elements of the protein.[18−20] It should be noted that in case the amide oscillators in random coil or $\alpha$-helical segments exhibit vibrational lifetimes very similar to either the $\alpha(-)$ or $\alpha(+)$ mode, an unambiguous distinction solely based on a kinetic analysis is not possible. The high-frequency band (blue curve) shown in the inset of Figure 2 has a non-negligible amplitude at around 1650 cm$^{-1}$, which likely originates from the amide I′ vibrations of random coil/helical elements that show a similar lifetime as the $\alpha(+)$ mode.

In a simulation study of the 11-residue $\beta$-hairpin peptide *trpzip2*, Jansen and Knoester found population transfer between the $\alpha(-)$ and $\alpha(+)$ modes of $\beta$-sheets,[28] but in this study, the transfer rate was found to be approximately a factor of 10 larger than that in the present study. The value of (7.1 ps)$^{-1}$ that we find for the exchange rate of AFPIII is in good agreement with the cross-relaxation rates of (5.26 ps)$^{-1}$ measured by Woutersen et al. for trialanine.[15] In this latter study, the energy-transfer dynamics were found to be completely determined by a subpicosecond component in the correlation function of the fluctuating coupling between the amide oscillators. It is thus conceivable that the cross-relaxation between the $\alpha(-)$ and $\alpha(+)$ modes in AFPIII results from fast conformational fluctuations of the $\beta$-sheets of the protein. We measured the temperature dependence of the exchange rate over an interval from 2 to 20 °C and found the exchange rate to vary only within the experimental uncertainty. This observation implies that the protein backbone remains relatively flexible over the investigated temperature range, even at temperatures approaching the freezing point of the solvent. This notion of highly flexible $\beta$-sheets is supported by the absence of detectable secondary structure in circular dichroism spectroscopy, while the X-ray diffraction structure of flash-frozen


dx.doi.org/10.1021/jp503481e | J. Phys. Chem. B XXXX, XXX, XXX−XXX

crystals with strongly suppressed dynamics reveals two $\beta$-sheets, a $\beta$-bridge, and two $3_{10}$ helices[18−20]

In the case of broad-band pumping, the anisotropy of $\alpha(+)$ shows a very fast decay that we can explain from the energy transfer between the $\alpha(-)$ and $\alpha(+)$ modes. Similar subpicosecond decays of the anisotropy have been observed before in infrared pump−probe experiments on the peptides apamin, scyllatoxin, and bovine pancreatic inhibitor.[4] In line with our interpretation, these fast decays have been assigned to energy transfer within the amide I′ vibrational manifold.[4] In the case of narrow-band excitation, the anisotropy dynamics of both the $\alpha(-)$ and the $\alpha(+)$ mode are quite slow because the transfer between these modes will negligibly contribute to the anisotropy decay. In the experiments of Figure 7b, only either of the two modes gets excited, and to get an effect of energy transfer on the anisotropy, the energy should not only be transferred to the unexcited mode but also back to the excited mode, which makes this contribution rather unimportant. The observed slow decay of the anisotropy can be ascribed to either molecular reorientation or to energy transfer between different modes $\alpha(-)$ or between different modes $\alpha(+)$. The first option can be ruled out in the present case considering the size of the protein and the relatively fixed orientation of the amide moiety in the peptide chain. The second option of energy transfer between different modes $\alpha(-)/\alpha(+)$ implies that there is a coupling between the modes leading to an excitonic manifold of delocalized $\alpha(-)$ states and an excitonic manifold of delocalized $\alpha(+)$ states. When either of the bands is excited, a set of excitonic states is populated that initially interferes constructively to an excited state for which the transition dipole moment is well aligned with the polarization of the pump pulse. The subsequent quantum interference and dephasing of the excitonic states will lead to a change of the orientation of the transition dipole moment and thus to a decay of the anisotropy. This type of quantum interference and dephasing has been discussed in ref 4 for the amide I modes of several other peptides and also for the case of coupled electronic states in ref 29. The interpretation of the anisotropy decay of Figure 7b in terms of dephasing of an excitonic manifold of $\alpha(-)/\alpha(+)$ states is further corroborated by inspection of the width of the spectral hole that is burned into the amide I′ absorption band upon excitation with a narrow-band pump pulse. A fit of a Lorentzian line shape function to the spectral hole obtained upon excitation of the $\alpha(+)$ mode at 1670 $\text{cm}^{-1}$ in Figure 3d yields a full width at half-maximum (fwhm) of approximately 12 $\text{cm}^{-1}$. This value is comparable to the bandwidth of the excitation pulse ($\Delta\nu_{\text{fwhm}} \approx 10$ $\text{cm}^{-1}$), which implies that the dephasing time of the $\alpha(+)$ states must occur on a time scale that is significantly longer than the duration of the excitation pulses. Previous work showed that the dephasing of excitonic amide I modes typically takes place with a time constant of $T_2 \approx 1$ ps,[4,6,30] thus making it indeed plausible that excitonic dephasing can lead to a decay of the anisotropy on a time scale of picoseconds, as observed in Figure 7b.

## 5. CONCLUSION

We have shown that the vibrational relaxation of the amide I′ band of a type-III antifreeze protein shows a pronounced frequency dependence, originating from the presence of two distinct amide I′ bands with lifetimes of 1.09 ± 0.01 and 3.21 ± 0.02 ps. From a two-dimensional spectroscopic experiment, it was found that the two bands are coupled and exchange population with a rate of $k_{B\to A} = (7.1 \pm 0.2\ \text{ps})^{-1}$. On the basis of this observation, we have assigned the observed components to the $\alpha(-)$ and $\alpha(+)$ modes of $\beta$-sheets. The influence of population exchange between the modes was found to have a large impact on the anisotropy dynamics obtained under broad-band excitation conditions, whereas the anisotropy dynamics of narrow-band pump experiments are rather insensitive to this aspect. The population exchange is likely enabled by the fast, (sub-)picosecond conformational fluctuations of the $\beta$-sheets. The exchange rate constant shows little variation over a temperature interval from 2 to 20 °C. This finding indicates that the protein backbone is flexible, even at temperatures near the freezing point (3.8 °C, $D_2O$). This notion is corroborated by the absence of detectable secondary structure in circular dichroism spectroscopy, while the X-ray diffraction structure of flash-frozen crystals with strongly suppressed dynamics reveals two $\beta$-sheets, a $\beta$-bridge, and two $3_{10}$ helices.

## APPENDIX

The rate equations for the population of the three states included in the model depicted in Figure 4 can be written in matrix form

$$\frac{\text{d}}{\text{d}t}\begin{pmatrix} N_A(t) \\ N_B(t) \\ N_0(t) \end{pmatrix} = \begin{pmatrix} -k_A - k_{A\to B} & k_{B\to A} & 0 \\ k_{A\to B} & -k_B - k_{B\to A} & 0 \\ k_A & k_B & 0 \end{pmatrix} \cdot \begin{pmatrix} N_A(t) \\ N_B(t) \\ N_0(t) \end{pmatrix} \tag{A1}$$

The rate equations are solved by finding the eigenvalues of the rate matrix in eq A1 with a given set of initial values $N_i(t = 0)$. In a subsequent step, the solutions to the rate equations $N_A(t)$, $N_B(t)$ are used to obtain associated spectral signatures $\sigma_A(\omega)$, $\sigma_B(\omega)$ from a least-squares solution of the following set of equations for every frequency point $\omega_j$

$$\begin{pmatrix} N_A(t_1, \omega_j) & N_B(t_1, \omega_j) \\ N_A(t_2, \omega_j) & N_B(t_2, \omega_j) \\ \multicolumn{2}{c}{\cdots} \\ N_A(t_n, \omega_j) & N_B(t_n, \omega_j) \end{pmatrix} \cdot \begin{pmatrix} \sigma_A(\omega_j) \\ \sigma_B(\omega_j) \end{pmatrix} = \begin{pmatrix} \Delta\alpha(t_1, \omega_j) \\ \Delta\alpha(t_2, \omega_j) \\ \cdots \\ \Delta\alpha(t_n, \omega_j) \end{pmatrix} \tag{A2}$$

Here, we have set $\sigma_0 = 0$ because of the subtraction of the thermal signal. The two steps are repeated in a minimization routine of the target function

$$\chi^2 = \sum_i \frac{(\Delta\alpha_{i,\text{iso}}(\omega, t) - (N_A(t)\cdot\sigma_A(\omega) + N_B(t)\cdot\sigma_B(\omega)))^2}{\epsilon_{i,\text{iso}}(\omega, t)^2} \tag{A3}$$

until the best match of the model with the experimental data points $\Delta\alpha_{i,\text{iso}}(\omega,t)$, weighted with the experimental uncertainties $\epsilon_{i,\text{iso}}(\omega,t)$, is found. The rates of vibrational relaxation to the ground state $k_A = 1/T_{1a}$ and $k_B = 1/T_{1b}$ and the rate of population transfer $k_{A\to B} = 1/T_{A\to B}$ are treated as free parameters in this routine. The rate of energy transfer in the reversed direction is constrained to obey the detailed balance condition $k_{A\to B}/k_{B\to A} = e^{-\Delta E/kT}$, where $k$, $T$, and $\Delta E$ denote Boltzman's constant, the sample temperature in Kelvin, and the energy gap between the two coupled amide modes of ∼35 $\text{cm}^{-1}$.

To construct the anisotropy decays associated with the two bands included in the model, we write the transient absorption


dx.doi.org/10.1021/jp503481e | J. Phys. Chem. B XXXX, XXX, XXX−XXX

changes obtained under parallel polarization of pump and probe pulses in the following way

$$\Delta\alpha_{\parallel}(\omega, t) = N_{A,\parallel}(t)\cdot\sigma_A(\omega) + N_{B,\parallel}(t)\cdot\sigma_B(\omega) \tag{A3}$$

Analogously, the transient absorption changes obtained for perpendicularly polarized light pulses can be written as

$$\Delta\alpha_{\perp}(\omega, t) = N_{A,\perp}(t)\cdot\sigma_A(\omega) + N_{B,\perp}(t)\cdot\sigma_B(\omega) \tag{A4}$$

Because $\sigma_A$ and $\sigma_B$ have been obtained from the fit of the isotropic data set $\Delta\alpha_{iso}$, we are able to use them in a least-squares decomposition of $\Delta\alpha_{\parallel}$ and $\Delta\alpha_{\perp}$ to obtain $N_{i,\parallel}$ and $N_{i,\perp}$. We use these quantities to construct the anisotropy decay $R_i(t)$ for both bands individually

$$R_i(t) = \frac{N_{i,\parallel} - N_{i,\perp}(t)}{N_{i,\parallel} + 2N_{i,\perp}(t)} \qquad i \in A, B \tag{A5}$$

## ■ ASSOCIATED CONTENT

### Ⓢ Supporting Information

Solvent-corrected temperature difference spectra of the amide I′ region and parameters of the calculation shown in Figure 6a,b of the paper. This material is available free of charge via the Internet at http://pubs.acs.org.

## ■ AUTHOR INFORMATION

### Corresponding Author

*E-mail: lotze@amolf.nl.

### Notes

The authors declare no competing financial interest.

## ■ ACKNOWLEDGMENTS

This work is part of the research program of the “Stichting voor Fundamenteel Onderzoek der Materie (FOM)”, which is financially supported by the “Nederlandse organisatie voor Wetenschappelijk Onderzoek (NWO)”. I.K.V. gratefully acknowledges The Netherlands Organisation for Scientific Research (NWO - VENI Grant: 700.10.406) and the European Union through the Marie Curie Fellowship program FP7-PEOPLE-2011-CIG (Contract No. 293788) for funding. Hinco Schoenmaker and Marco Konijnenburg are gratefully acknowledged for technical support during the project.

## ■ REFERENCES

(1) Barth, A. Infrared Spectroscopy of Proteins. *Biochim. Biophys. Acta* **2007**, *1767*, 1073−1101.

(2) Bandekar, J.; Krimm, S. Vibrational Analysis of Peptides, Polypeptides, and Proteins. VI. Assignment of β-Turn Modes in Insulin and Other Proteins. *Biopolymers* **1980**, *19*, 31−36.

(3) Torii, H.; Tasumi, M. Model Calculations on the Amide-I Infrared Bands of Globular Proteins. *J. Chem. Phys.* **1992**, *96*, 3379−3387.

(4) Hamm, P.; Lim, M.; Hochstrasser, R. M. Structure of the Amide I Band of Peptides Measured by Femtosecond Nonlinear-Infrared Spectroscopy. *J. Phys. Chem. B* **1998**, *102*, 6123−6138.

(5) Manor, J.; Mukherjee, P.; Lin, Y.-S.; Leonov, H.; Skinner, J. L.; Zanni, M. T.; Arkin, I. T. Gating Mechanism of the Influenza A M2 Channel Revealed by 1D and 2D IR Spectroscopies. *Structure* **2009**, *17*, 247−254.

(6) Woys, A. M.; Lin, Y.-S.; Reddy, A. S.; Xiong, W.; de Pablo, J. J.; Skinner, J. L.; Zanni, M. T. 2D IR Line Shapes Probe Ovispirin Peptide Conformation and Depth in Lipid Bilayers. *J. Am. Chem. Soc.* **2010**, *132*, 2832.

(7) Mukherjee, P.; Kass, I.; Arkin, I. T.; Zanni, M. T. Picosecond Dynamics of a Membrane Protein Revealed by 2D IR. *Proc. Natl. Acad. Sci. U.S.A.* **2006**, *103*, 3528−3533.

(8) Demirdöven, N.; Cheatum, C. M.; Chung, H. S.; Khalil, M.; Knoester, J.; Tokmakoff, A. Two-Dimensional Infrared Spectroscopy of Antiparallel β-Sheet Secondary Structure. *J. Am. Chem. Soc.* **2004**, *126*, 7981−7990.

(9) Smith, A. W.; Lessing, J.; Ganim, Z.; Peng, C. S.; Tokmakoff, A.; Roy, S.; Jansen, T. L. C.; Knoester, J. Melting of a β-Hairpin Peptide Using Isotope-Edited 2D IR Spectroscopy and Simulations. *J. Phys. Chem. B* **2010**, *114*, 10913−10924.

(10) Lessing, J.; Roy, S.; Reppert, M.; Baer, M.; Marx, D.; Jansen, T. L. C.; Knoester, J.; Tokmakoff, A. Identifying Residual Structure in Intrinsically Disordered Systems: A 2D IR Spectroscopic Study of the GVGXPGVG Peptide. *J. Am. Chem. Soc.* **2012**, *134*, 5032−5035.

(11) Ghosh, A.; Qiu, J.; DeGrado, W. F.; Hochstrasser, R. M. Tidal Surge in the M2 Proton Channel, Sensed by 2D IR Spectroscopy. *Proc. Natl. Acad. Sci. U.S.A.* **2011**, *108*, 6115−6120.

(12) Remorino, A.; Korendovych, I. V.; Wu, Y.; DeGrado, W. F.; Hochstrasser, R. M. Residue-Specific Vibrational Echoes Yield 3D Structures of a Transmembrane Helix Dimer. *Science* **2011**, *332*, 1206−1209.

(13) Middleton, C. T.; Buchanan, L. E.; Dunkelberger, E. B.; Zanni, M. T. Utilizing Lifetimes to Suppress Random Coil Features in 2D IR Spectra of Peptides. *J. Phys. Chem. Lett.* **2011**, *2*, 2357−2361.

(14) Woutersen, S.; Mu, Y.; Stock, G.; Hamm, P. Hydrogen-Bond Lifetime Measured by Time-Resolved 2D-IR Spectroscopy: N-Methylacetamide in Methanol. *Chem. Phys.* **2001**, *266*, 137−147.

(15) Woutersen, S.; Mu, Y.; Stock, G.; Hamm, P. Subpicosecond Conformational Dynamics of Small Peptides Probed by Two-Dimensional Vibrational Spectroscopy. *Proc. Natl. Acad. Sci. U.S.A.* **2001**, *98*, 11254−11258.

(16) Volkov, V.; Hamm, P. A Two-Dimensional Infrared Study of Localization, Structure, and Dynamics of a Dipeptide in Membrane Environment. *Biophys. J.* **2004**, *87*, 4213−4225.

(17) Yeh, Y.; Feeney, R. E. Antifreeze Proteins: Structures and Mechanisms of Function. *Chem. Rev.* **1996**, *96*, 601−618.

(18) Sönnichsen, F. D.; DeLuca, C. I.; Davies, P. L.; Sykes, B. D. Refined Solution Structure of Type III Antifreeze Protein: Hydrophobic Groups May Be Involved in the Energetics of the Protein−Ice Interaction. *Structure* **1996**, *4*, 1325−1337.

(19) Antson, A. A.; Smith, D. J.; Roper, D. I.; Lewis, S.; Caves, L. S.; Verma, C. S.; Buckley, S. L.; Lillford, P. J.; Hubbard, R. E. Understanding the Mechanism of Ice Binding by Type III Antifreeze Proteins. *J. Mol. Biol.* **2001**, *305*, 875−889.

(20) Salvay, A. G.; Gabel, F.; Pucci, B.; Santos, J.; Howard, E. I.; Ebel, C. Structure and Interactions of Fish Type III Antifreeze Protein in Solution. *Biophys. J.* **2010**, *99*, 609−618.

(21) Boyd, R. W.; Mukamel, S. Origin of Spectral Holes in Pump−Probe Studies of Homogeneously Broadened Lines. *Phys. Rev. A* **1984**, *29*, 1973−1983.

(22) Woutersen, S.; Bakker, H. J. Coherent Coupling in Frequency-Resolved Pump−Probe Spectroscopy. *J. Opt. Soc. Am. B* **2000**, *17*, 827−832.

(23) Hamm, P. Coherent Effects in Femtosecond Infrared Spectroscopy. *Chem. Phys.* **1995**, *200*, 415−429.

(24) Wynne, K.; Hochstrasser, R. The Theory of Ultrafast Vibrational Spectroscopy. *Chem. Phys.* **1995**, *193*, 211−236.

(25) Cervetto, V.; Helbing, J.; Bredenbeck, J.; Hamm, P. Double-Resonance versus Pulsed Fourier Transform Two-Dimensional Infrared Spectroscopy: An Experimental and Theoretical Comparison. *J. Chem. Phys.* **2004**, *121*, 5935−5942.

(26) Hamm, P.; Lim, M.; DeGrado, W. F.; Hochstrasser, R. M. The Two-Dimensional IR Nonlinear Spectroscopy of a Cyclic Penta-Peptide in Relation to its Three-Dimensional Structure. *Proc. Natl. Acad. Sci. U.S.A.* **1999**, *96*, 2036−2041.

(27) Miyazawa, T. Perturbation Treatment of the Characteristic Vibrations of Polypeptide Chains in Various Configurations. *J. Chem. Phys.* **1960**, *32*, 1647−1652.



dx.doi.org/10.1021/jp503481e | *J. Phys. Chem. B* XXXX, XXX, XXX−XXX

(28) la Cour Jansen, T.; Knoester, J. Two-Dimensional Infrared Population Transfer Spectroscopy for Enhancing Structural Markers of Proteins. *Biophys. J.* **2008**, *94*, 1818−1825.
(29) Wynne, K.; Hochstrasser, R. Coherence Effects in the Anisotropy of Optical Experiments. *Chem. Phys.* **1993**, *171*, 179−188.
(30) Hamm, P.; Lim, M.; DeGrado, W. F.; Hochstrasser, R. M. Stimulated Photon Echoes from Amide I Vibrations. *J. Phys. Chem. A* **1999**, *103*, 10049−10053.